Cell Reports
Physical Science

CellPress
OPEN ACCESS

Article

A solution-based route to compositionally complex metal oxide structures using high-entropy layered double hydroxides

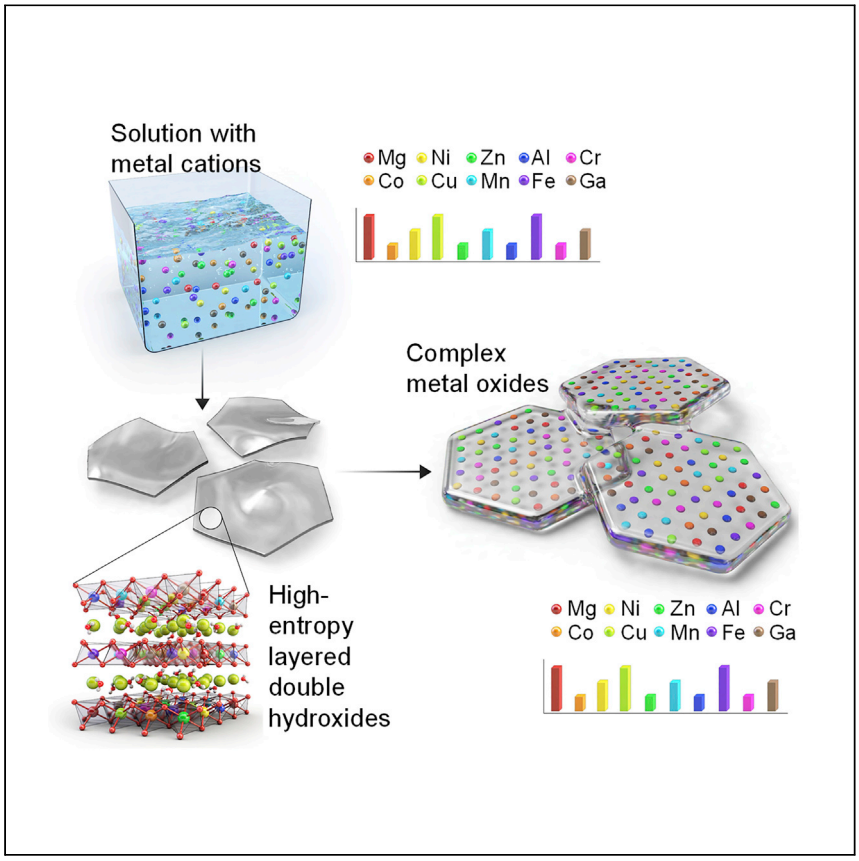

A solution-based synthesis of compositionally complex metal oxides is challenging. Kim et al. prepare high-entropy layered double hydroxides containing 10 different metal cations by a solution-based route. The high-entropy materials are transformed into compositionally complex metal oxides with controlled compositions by simple heat treatments.

Miri Kim, Inseon Oh, Hyunkyung Choi, ..., Chul Sung Kim, Jung-Woo Yoo, Seungho Cho

cskim@kookmin.ac.kr (C.S.K.)
jwyoo@unist.ac.kr (J.-W.Y.)
scho@unist.ac.kr (S.C.)

Highlights

Formation of high-entropy layered double hydroxides with 10 different metal cations

Solution-based preparation of composition-controlled complex metal oxides

Kim et al., Cell Reports Physical Science 3, 100702
January 19, 2022
https://doi.org/10.1016/j.xcrp.2021.100702

Cell Reports
Physical Science

CellPress
OPEN ACCESS

Article

A solution-based route to compositionally complex metal oxide structures using high-entropy layered double hydroxides

Miri Kim,[1,3] Inseon Oh,[1,3] Hyunkyung Choi,[2] Wonsik Jang,[1] Jaejung Song,[1] Chul Sung Kim,[2,*] Jung-Woo Yoo,[1,*] and Seungho Cho[1,4,*]

SUMMARY

Although complex metal oxides with tailored compositions are increasingly in demand for applications in advanced technologies, their preparation by solution-based routes, which are typically low cost and easy to scale up, is challenging. Here, we report high-entropy layered double hydroxides (HE-LDHs) having complex compositions as precursors for complex metal oxides. Furthermore, we reveal that the ionic radii are the key factors determining the incorporation of the metal cations into the hydroxide layers, which can contain up to 10 different kinds of metal cations simultaneously having a metal cation ratio inherited from the reaction solution. Furthermore, spinel-based complex oxides can be prepared by heat treating the HE-LDHs in air, and their metal cation ratios are maintained over expansive heat-treatment temperatures (up to 1,200°C). Therefore, the results reveal that complex oxides with tailored compositions can be prepared using solution-based approaches, enabling the large-scale fabrication of oxides with precisely controlled physicochemical properties for various applications.

INTRODUCTION

Complex metal oxides (i.e., metal oxides with complex compositions) have unique physicochemical properties that cannot be achieved by metal oxides with simple compositions. Hence, complex oxides have attracted attention in a wide range of fields such as electronics, magnetic materials, capacitors, actuators, memory devices, batteries, and solar cells.[1–11] To date, complex oxide films and nanostructures have been prepared mainly by physical vapor deposition such as pulsed laser deposition (PLD) and molecular beam epitaxy (MBE) because these methods allow precise control over the composition of the deposited materials. In contrast, solution-based syntheses have advantages over physical vapor deposition, particularly concerning the applications of the prepared materials. In particular, these methods are more economical because they are energy efficient and easy to scale-up. On the other hand, in solution-based methods, there is little control over the material composition. For example, even if reaction solutions contain diverse metal cations, during the formation of thermodynamically stable solid-state phases, only the metal cations needed to construct these stable crystal phases are taken from solution, thus excluding other solution components.[12] Furthermore, as the compositional complexity of a solution-based growth system increases, achieving the desired material compositions becomes more challenging.

[1]Department of Materials Science and Engineering, Ulsan National Institute of Science and Technology (UNIST), Ulsan 44919, Republic of Korea

[2]Department of Physics, Kookmin University, Seoul 02707, Republic of Korea

[3]These authors contributed equally

[4]Lead contact

*Correspondence: cskim@kookmin.ac.kr (C.S.K.), jwyoo@unist.ac.kr (J.-W.Y.), scho@unist.ac.kr (S.C.)

https://doi.org/10.1016/j.xcrp.2021.100702

Interestingly, however, layered double hydroxides (LDHs), which are ionic lamellar solids, can be readily prepared by solution-based synthetic methods and can contain several combinations of metal cations.[13,14] Moreover, LDHs are characterized by the dispersion (rather than segregation) of metal cations throughout the metal hydroxide layers.[15,16] Therefore, because of this high degree of compositional freedom, LDHs themselves have been used in a variety of applications, for example, as catalysts, supercapacitors, and battery, solar cell, and sensor components, as well as for energy conversion applications.[17–23] LDHs can also be used as precursors for functional mixed metal oxides (MMOs).[24]

To date, the discussion of the composition of LDHs has mainly focused on their applications. Moreover, studies investigating the control of LDH composition remain rare. Furthermore, although LDHs are known for their compositional variety, not all types of metal cations can be contained in the metal hydroxide layers. However, currently, the rules behind the choice of metal cation remain unknown. This is crucial information because the composition of the LDH strongly influences its physicochemical properties and those of any derived MMOs.

Therefore, in this study, we investigated the formation of LDHs to reveal the factors determining metal cation incorporation into the metal hydroxide layers of LDHs and to show the possibility of forming high-entropy LDHs (HE-LDHs) containing various metal cations. Recently, high-entropy materials,[25] such as alloys,[26,27] oxides,[28–30] and carbides,[31] have received great attention because of their promising properties. High-entropy materials are characterized as having five or more elements homogeneously distributed in a single phase with random occupancy.[32] These materials could have properties tailored by varying the multi-component structures having maximized configurational entropy.[25,28] Furthermore, because of their unique properties (variation in components, crystal structure, and stoichiometry) and cocktail effects, high-entropy materials have been investigated intensely for various applications in processes such as methanol oxidation,[25] the oxygen-evolution reaction,[32–34] and Li-ion battery technology.[30,35–38] In addition, the compositional controllability and metal cation dispersibility of LDHs are further investigated. Furthermore, the relationships between the crystal structures and compositions of LDHs and MMOs derived by heat treatment were studied. We found that the metal cations were uniformly distributed in the LDHs and the ratios of metal cations in the reaction solution were preserved in the LDHs and calcined products, suggesting their applications as high-temperature-resistant information storage materials (Figure 1).

RESULTS AND DISCUSSION

Preparation and characterization of high-entropy LDHs

LDHs are composed of octahedrons having metal cations at the centers (Figure 1). Figure 2 shows a structure field map with the ionic radii of various metal cations. We conducted co-precipitation with combinations of all the metal cations in the map except the noble metals marked by green triangles and metal cations that cannot be used in solution-based methods. Combinations of metal cations (pairs of 2+ and 3+ cations) marked by the red rhombuses resulted in the formation of LDHs. Notably, the metal cations in the shaded area (i.e., those having ionic radii less than 98 pm) in the map formed LDHs. Based on Pauling's first rule, if the ionic radius of OH^- is 133 pm with a coordination number of 3, a cation with an ionic radius between 55 pm and 98 pm should be stable in the metal hydroxide octahedron.[39] However, for cation ionic radii larger than 98 pm, higher coordination geometries should be preferred, thus making it difficult to form the octahedral structure. The

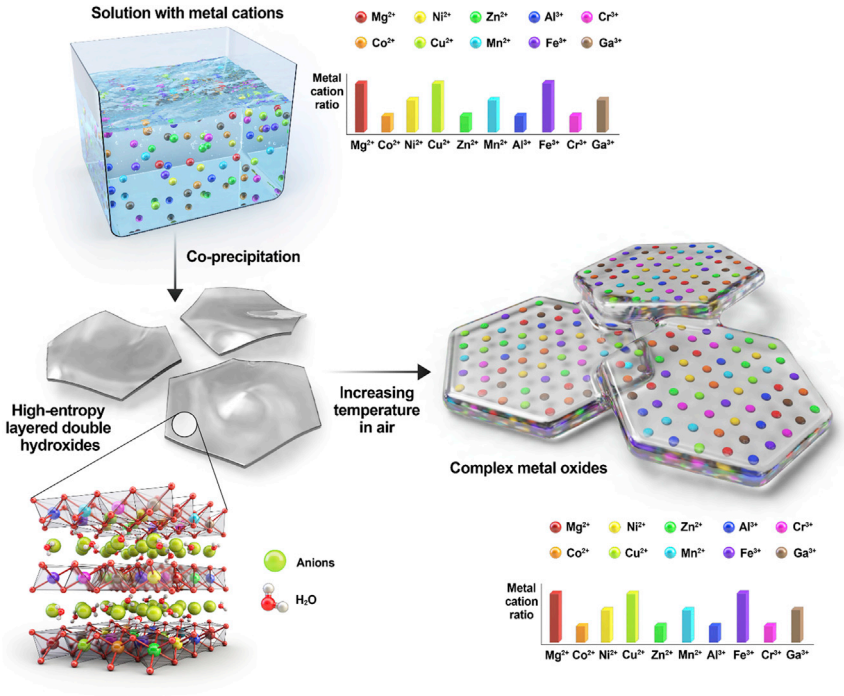

Figure 1. Schematic illustration of HE-LDHs and complex metal oxides

Schematic of the formation of HE-LDHs from solution with various metal cations and the transformation of the HE-LDHs to complex metal oxides.

metal cations that could not occupy the octahedral centers in this study have ionic radii greater than 98 pm. This trend indicates that the ionic radius of the metal cation is the deciding factor in the formation of the hydroxide octahedrons of LDHs.

Next, we synthesized HE-LDH powder samples from aqueous solutions containing equimolar amounts of 10 metal cations (0.07 M each) of Mg, Co, Al, Ni, Fe, Cr, Cu, Zn, Mn, and Ga (i.e., the 10 metal cations that could be successfully incorporated into the metal hydroxide layers; Figure 2). The X-ray diffraction (XRD) patterns of the as-prepared powders (Figure 3Ai) are typical of LDH materials (ICDD 00-014-0191), with peaks corresponding to the (003), (006), (009), (015), (110), and (113) planes. No other crystalline phases were detected. The scanning electron microscopy (SEM) image (Figure 3Bi) shows that the precipitates have typical sheet-like morphologies of LDHs. No other morphologies were observed. Interestingly, the inductively coupled plasma optical emission spectroscopy (ICP-OES) results show that the as-prepared HE-LDHs inherited the metal cation ratios of the reaction solutions (Figure 3Ci). The transmission electron microscopy (TEM) images of the HE-LDHs (Figures S1A and S1B) show that the LDHs are highly crystalline and stacked in layers. Note that the white boxed area in the scanning TEM high-angle annular dark-field (STEM-HAADF) image in Figure S2A (200-nm scale bar) corresponds to the area of the STEM-HAADF image in Figure 3D (20-nm scale bar). The STEM-HAADF images and the corresponding energy dispersive X-ray spectroscopy (EDS) elemental maps (Figure 3D; Figure S2A) reveal that the 10 different metal cations were uniformly distributed throughout the structures.

The Fourier transform infrared (FTIR) spectrum of the HE-LDHs is shown in Figure S3. The OH stretching vibrations of the octahedral hydroxide layer and H_2O molecules

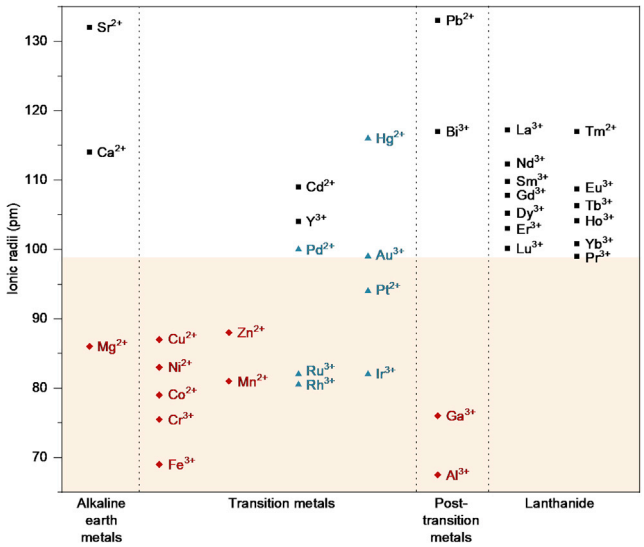

Figure 2. Structure field map of layered double hydroxide structures

Red rhombuses, LDHs with the corresponding metal cations were formed; black squares, LDHs with the corresponding metal cations were not formed; green triangles, noble metals.

in the interlayer space appear around 3,400 cm^{-1}, and the hydrogen bonding of H_2O molecules to CO_3^{2-} ions in the interlayer space results in a shoulder at 2,960 cm^{-1}.[40,41] The OH vibrations of interlayer H_2O molecules are characterized by the band at 1,640 cm^{-1},[42,43] and the bands at 1,510 and 1,360 cm^{-1} are characteristics of the stretching vibrations of interlayer CO_3^{2-} ions.[44] The M-O lattice vibrations are observed as a band below 800 cm^{-1}.[45] Furthermore, the oxidation state of Fe and its chemical environment in the HE-LDHs were investigated using Mössbauer spectroscopy (Figure S5). At ambient temperature, the spectrum is an electric quadrupole doublet of Fe^{3+} with a quadrupole splitting (ΔE_Q) of 0.67 mms^{-1}, isomer shift (δ) of 0.22 mms^{-1}, and line width (Γ) of 0.43 mms^{-1}. Combined with the EDS elemental mapping results, the Mössbauer data indicate that the metal cations are homogeneously distributed in the single-phase compound.

Preparation and characterization of compositionally complex metal oxides derived from high-entropy LDHs

Next, the structural and chemical changes to the HE-LDHs on heat treatment in air were investigated. After heat treatment at 300°C, the peaks corresponding to LDH disappeared from the XRD patterns, and broad peaks corresponding to the (111), (220), (311), (400), (422), (511), and (440) planes of spinel oxides peaks (ICDD 00-050-0235) appeared (Figure 3Aii). This result indicates that the layered structure of the HE-LDHs collapses as a result of dehydroxylation[46] and small spinel oxide crystal grains are formed. Nevertheless, the outer shapes of the calcined structures remained similar to those of the as-prepared HE-LDHs (Figure 3Bii).

The HE-LDHs prepared in this study are characterized as having a good dispersion of the different metal cations without segregation, and crucially, the cation ratios of the HE-LDHs were maintained after heat treatment (Figure 3Cii). In addition, the transformation of the HE-LDHs into metal oxides required a lower energy of formation than those of conventional solid-state reactions, as shown by the appearance of reflections corresponding to the spinel structure after calcination at 300°C (Figure 3Aii). This result is probably because of the small diffusion distances of the constituent cations in the LDHs.

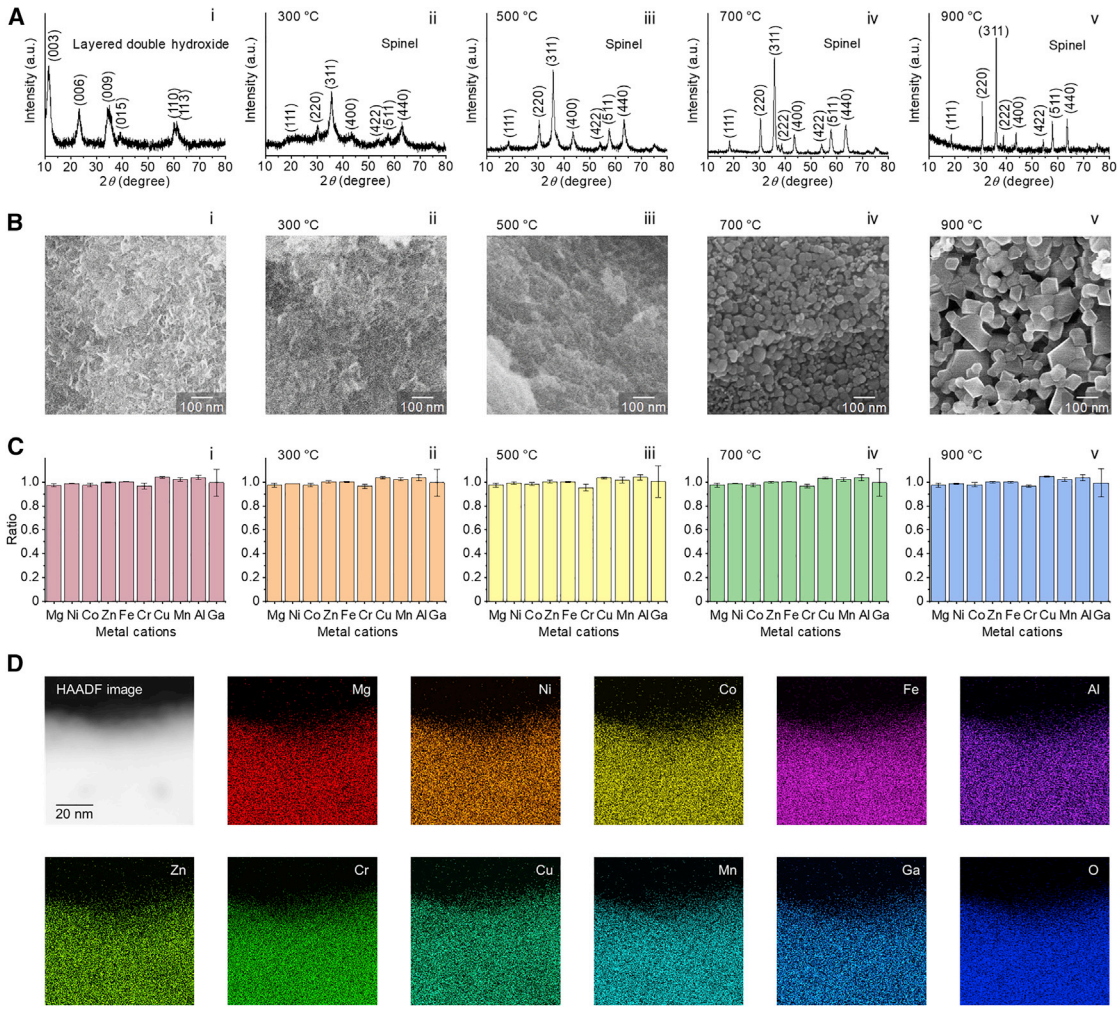

Figure 3. Characterization of HE-LDHs and mixed metal oxides with equimolar metal cations

(A–C) X-ray diffraction patterns (A), scanning electron microscopy images (B), and metal cation ratios (C) obtained by inductively coupled plasma optical emission spectroscopy of (i) HE-LDHs prepared from a solution containing Mg, Ni, Co, Fe, Al, Zn, Cr, Cu, Mn, and Ga cations, and their products obtained by calcination at (ii) 300°C, (iii) 500°C, (iv) 700°C, and (v) 900°C. The error bars indicate the standard deviations of the metal cation ratios determined by repeating the measurements thrice.

(D) High-angle annular dark-field scanning transmission electron microscopy image of HE-LDH particles containing various metal cations and the corresponding energy-dispersive X-ray spectroscopy elemental maps for Mg, Ni, Co, Fe, Al, Zn, Cr, Cu, Mn, Ga, and O.

As the calcination temperature was increased through 500°C, 700°C, and 900°C, the peaks corresponding to the spinel structure became sharper in the XRD patterns, suggesting that the size of the crystallites or grains increased (Figures 3Aiii–3Av). Because the ionic radius range for LDH metal cations is shared with that for metal cations of spinels[47], the LDHs could be transformed to spinel oxides by heat treatment in air. In particular, heat treatment at 500°C did not lead to significant changes in morphology (Figure 3Biii), but heat treatment at 700°C resulted in the formation of particulates (grains) (Figure 3Biv), and these crystal grains further grew after calcination at 900°C (Figure 3Bv). These observations are consistent with the reduction in peak broadness of the XRD patterns with increasing temperature because of the growth of the crystal grains (Figure 3A). At certain temperatures, the crystal structures changed, but the outer morphology did not change significantly. However, with a further increase in the calcination temperature, the

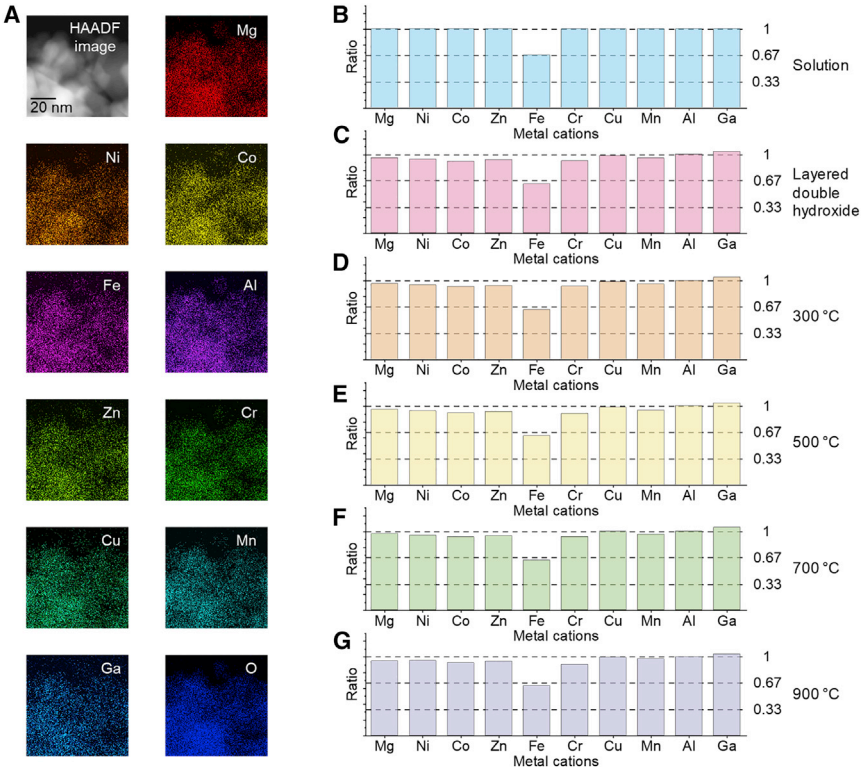

Figure 4. Characterization of MMOs heat treated at 700°C containing ten different metal cations in equimolar quantities and HE-LDHs and MMOs containing nine different metal cations in equimolar ratios and Fe cations in two-thirds the molar ratio of the other components

(A) High-angle annular dark-field scanning transmission electron microscopy image of powder containing various metal cations heat treated at 700°C and the corresponding energy-dispersive X-ray spectroscopy elemental maps for Mg, Ni, Co, Fe, Al, Zn, Cr, Cu, Mn, Ga, and O.

(B) The ratio of metal cations ionized in solution.

(C–G) Metal cation ratios obtained by inductively coupled plasma optical emission spectroscopy on HE-LDHs prepared from the solution (C) and metal oxides prepared by calcination of the HE-LDHs at 300°C (D), 500°C (E), 700°C (F), and 900°C (G).

morphologies and dimensions of the samples changed because of the growth of the grains having the spinel structure. The TEM images of the samples treated at 700°C (Figures S1C and S1D) show the enlarged spinel grains. Despite this morphological change, the metal cation ratios inherited from the solution were maintained after heat treatment at high temperatures (Figure 3C). Moreover, the STEM-HAADF image and the corresponding EDS elemental maps of the sample treated at 700°C (Figure 4A; Figure S2B) indicate that the 10 different metal cations were uniformly distributed in the structures without elemental segregation. Mg, Ni, Co, Fe, Al, Zn, Cr, Cu, Mn, and Ga have been reported as constituent elements of spinel structures.[48–50] Moreover, recently, high-entropy spinel oxides containing Co, Cr, Fe, Mn, and Ni[51] and spinels containing Mg, Ti, Zn, Cu, and Fe[30] have been reported. In the crystals, the entropic contributions to the free energy promote thermodynamic stability. As the number of components increases, the configurational entropy increases; $\Delta S_{conf} = R \ln n$, where R is the ideal gas constant and n is the number of components (in our case, n = 10).[25] The configurational entropy can regulate the normal-to-inverse transformation in spinel structures.[52] Therefore, single-phase spinel oxides containing 10 different metal cations can form.

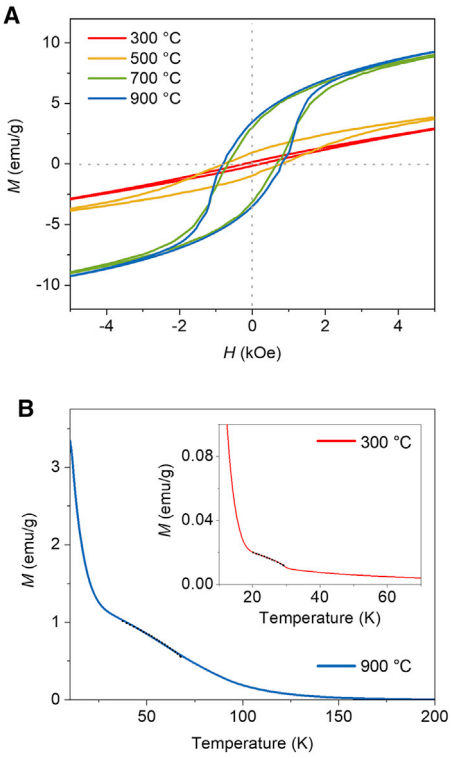

Figure 5. Magnetic properties of MMOs
(A) Hysteresis curves of MMOs prepared at 300°C, 500°C, 700°C, and 900°C measured at 10 K.
(B) Temperature-dependent magnetization of MMOs prepared at 300°C and 900°C.

The thermal decomposition of the HE-LDHs was further studied by simultaneous differential scanning calorimetry and thermogravimetric analysis (Figure S4). Between 30°C and 170°C, a mass loss was observed that corresponds to the removal of H_2O molecules from the interlayer space. Between 170°C and 300°C, a mass loss corresponding to the dehydroxylation of the hydroxide layer and extraction of the interlayer anions was observed. These changes indicate the transformation of the LDHs to MMOs. The third mass loss occurred between 300°C and 500°C and was a result of the total dehydroxylation and ejection of residues in the interlayer; this loss led to the collapse of the layered structures. There was also a slight mass loss above 500°C, and it can be ascribed to the elimination of residues from the mixed oxides.[53,54] Overall, the HE-LDHs lost 32.17% of their initial mass as a result of dehydroxylation and the removal of interlayer anions and water molecules.

Magnetic properties of complex metal oxides

Figure 5A shows the magnetic hysteresis curves of the MMOs measured at 10 K with an increase in the annealing temperature from 300°C to 900°C. The coercive field (H_C) and the remanent magnetization (M_R) increased significantly with an increase in the annealing temperatures of the HE-LDHs. For instance, the value of H_C for the sample annealed at 300°C was approximately 210 Oe, but that for the sample annealed at 700°C was 800 Oe. The temperature-dependent magnetization of the MMOs shown in Figure 5B indicates the coexistence of paramagnetic and ferromagnetic behavior at low temperatures. The Curie temperature (T_C) for the ferromagnetic components was estimated using mean field theory, $M \propto (T_C - T)^{1/2}$. The obtained values for the annealed samples at 300°C and 900°C are 34.2 and 80.7 K, respectively. The magnetic hysteresis curves of the samples treated at various annealing temperatures are displayed in Figure S6. These results indicate that the improved crystallinity with an increase in annealing temperature enhances the

ferromagnetic properties (e.g., H_C, M_R, and T_C) because the increase in crystallinity intensifies the long-range ferromagnetic order and strong exchange interactions in the MMOs.

Metal cation ratio control of high-entropy LDHs and complex metal oxides

To confirm the controllability over the metal cation ratios in the HE-LDHs and oxide derivatives, a control experiment was conducted. HE-LDHs were prepared from a solution containing Fe cations in a molar ratio equal to two-thirds of those of the other cations (Mg, Co, Al, Ni, Cr, Cu, Zn, Mn, and Ga; Figure 4B). An XRD analysis revealed that the HE-LDHs had formed successfully (Figure S7A). Furthermore, as in the case of equimolar metal cations (Figure 3), the HE-LDHs were transformed into spinel oxides after heat treatment in air (Figures S7B–S7E). In addition, the ICP-OES results for the LDH samples show that the molar ratios of cations of the reaction solution were preserved in the HE-LDHs (Figure 4C). Additionally, the metal ratios were maintained after heat treatment (Figures 4D–4G). Thus, the results indicate that the control over the composition of LDHs and derived metal oxides can be achieved by simply controlling the metal cation ratios of the reaction solution. Therefore, this solution-based method allows the preparation of complex metal oxides with desired compositions.

The exponential increase in the amount of electronic data in this information age means that there is an increasing need for data storage and processing.[55] Thus, we propose that high-entropy materials could be used as information storage media in the future. Crucially, the HE-LDH formation process is simple and achieved under ambient conditions, thus enabling large-scale production. Furthermore, because various metal cations can be uniformly distributed without segregation in the HE-LDHs[56] and their compositions can be precisely controlled, an individual LDH particle can contain information coded by the cation ratio. For example, if five distinct states of "add (ratio level 1)," "add (ratio level 2)," "add (ratio level 3)," "add (ratio level 4)," and "subtract (ratio level 0)" for each of 10 independent choices of metal are chosen, the number of combinations approaches 10^7. Moreover, the information stored in the HE-LDHs or oxide derivatives was not significantly affected by high-temperature treatment, as shown in Figures 3C and 4 (up to 1,200°C; Figure S8). By use of currently available techniques, information decoding could be achieved by quantitative analysis methods such as ICP-OES. Importantly, only extremely small amounts of the powder (or, in principle, a part of an individual LDH particle) would be needed for decoding because of the uniform distribution of cations in the structures. However, in the future, if a simpler quantitative analysis method were developed, information stored in the HE-LDHs or oxide derivatives could be decoded in a simpler fashion.

Figure 6 shows the metal cation ratio retention of the samples treated at high temperatures. Each metal cation ratio is close to that of the HE-LDHs at 23°C (i.e., close to 100% retention) over a wide range of temperatures. Thus, despite the use of heat treatment for morphology, crystallinity, crystallographic grain size, and vacancy control, the metal ratio was retained in the complex metal oxides. Therefore, the complex metal oxides derived from HE-LDHs have tailored compositions and structural properties, which makes them suitable for a wide range of applications.

In summary, we investigated LDH formation to identify the factors determining metal cation incorporation into the metal hydroxide layers of LDHs. Metal cations satisfying the ionic radius criterion can be incorporated into the LDH structures simultaneously. Thus, we prepared HE-LDHs containing Mg, Co, Al, Ni, Fe, Cr, Cu, Zn, Mn,

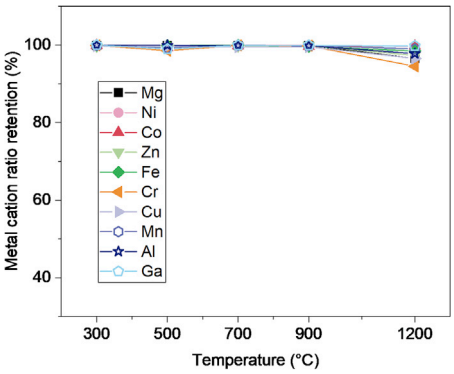

Figure 6. Metal cation ratio retention of MMOs

Retention of metal cation ratio of HE-LDHs derived metal oxides as a function of temperature.

and Ga uniformly distributed in the single-phase structures. Furthermore, their metal cation ratios were inherited from the reaction solutions and were maintained at high temperatures. Therefore, complex spinel oxides with controlled compositions can be prepared by using this solution-based method. In addition to the formation of HE-LDH powders, HE-LDH films can be deposited on substrates by layer-by-layer deposition or direct growth. Moreover, the range of possible cation radii can be extended by choosing other metal hydroxide precursors. Consequently, the precursor transformation approach described here provides a new avenue for the large-scale fabrication of advanced materials having tunable functional properties for various applications.

EXPERIMENTAL PROCEDURES

Resource availability

Lead contact

Further information and requests for resources and reagents should be directed to and will be fulfilled by the lead contact, Seungho Cho (scho@unist.ac.kr).

Materials availability

All materials generated in this study are available from the lead contact without restriction.

Data and code availability

The authors declare that data supporting the results of this study are available in the main text and supplemental information. Further information and requests for additional data should be directed to the lead contact.

Materials

Magnesium nitrate hexahydrate [$Mg(NO_3)_2 \cdot 6H_2O$, ≥99.0%], aluminum nitrate nonahydrate [$Al(NO_3)_3 \cdot 9H_2O$, ≥99.0%], cobalt nitrate hexahydrate [$Co(NO_3)_2 \cdot 6H_2O$, ≥99.0%], iron nitrate nonahydrate [$Fe(NO_3)_3 \cdot 9H_2O$, ≥99.0%], nickel nitrate hexahydrate [$Ni(NO_3)_2 \cdot 6H_2O$, ≥99.0%], copper nitrate trihydrate [$Cu(NO_3)_2 \cdot 3H_2O$, ≥99.0%], chromium nitrate nonahydrate [$Cr(NO_3)_3 \cdot 9H_2O$, ≥99.0%], zinc nitrate hexahydrate [$Zn(NO_3)_2 \cdot 6H_2O$, ≥99.0%], manganese nitrate tetrahydrate [$Mn(NO_3)_2 \cdot 4H_2O$, ≥99.0%], gallium nitrate hydrate [$Ga(NO_3)_3 \cdot H_2O$, ≥99.0%], lanthanum nitrate hexahydrate [$La(NO_3)_3 \cdot 6H_2O$, ≥99.99%], neodymium nitrate hexahydrate [$Nd(NO_3)_3 \cdot 6H_2O$, ≥99.9%], europium nitrate pentahydrate [$Eu(NO_3)_3 \cdot 5H_2O$, ≥99.9%], gadolinium nitrate hexahydrate [$Gd(NO_3)_3 \cdot 6H_2O$, ≥99.9%], terbium nitrate pentahydrate [$Tb(NO_3)_3 \cdot 5H_2O$, ≥99.9%], dysprosium nitrate hydrate [$Dy(NO_3)_3 \cdot H_2O$, ≥99.9%], holmium nitrate pentahydrate

[$Ho(NO_3)_3 \cdot 5H_2O$, ≥99.9%], erbium nitrate pentahydrate [$Er(NO_3)_3 \cdot 5H_2O$, ≥99.9%], thulium nitrate pentahydrate [$Tm(NO_3)_3 \cdot 5H_2O$, ≥99.9%], ytterbium nitrate pentahydrate [$Yb(NO_3)_3 \cdot 5H_2O$, ≥99.9%], lutetium nitrate hydrate [$Lu(NO_3)_3 \cdot H_2O$, ≥99.9%], strontium nitrate [$Sr(NO_3)_2$, ≥99.0%], samarium nitrate hexahydrate [$Sm(NO_3)_3 \cdot 6H_2O$, ≥99.9%], lead nitrate [$Pb(NO_3)_2$, ≥99.0%], cadmium nitrate tetrahydrate [$Cd(NO_3)_2 \cdot 4H_2O$, ≥98.0%], praseodymium nitrate hexahydrate [$Pr(NO_3)_3 \cdot 6H_2O$, ≥99.9%], bismuth nitrate pentahydrate [$Bi(NO_3)_3 \cdot 5H_2O$, ≥98.0%], sodium carbonate [Na_2CO_3, ≥99.0%], and sodium hydroxide [NaOH, ≥98%] were used. All chemicals were purchased from Sigma-Aldrich, and they were used without further purification.

Synthesis of HE-LDHs and MMOs

To prepare the HE-LDHs, 0.007 mol of the nitrate salt of each metal was dissolved in 100 mL deionized water (solution A). Then, 0.2 mol of NaOH and 0.08 mol of Na_2CO_3 were dissolved in 200 mL deionized water to obtain an aqueous 1 M NaOH and 0.4 M Na_2CO_3 solution (solution B). Then, solution B was slowly poured into solution A until pH 10 was reached, and the resultant solution was maintained at 60°C for 24 h. The precipitates were washed with deionized water and ethanol using a centrifuge and vortex mixer. The precipitates were dried at 60°C for 24 h, and then the powders were collected. To prepare metal oxides containing various metal cations, the LDH powders were placed in alumina boats and calcined at 300°C, 500°C, 700°C, 900°C, or 1,200°C for 1 h in a box furnace. The heating rates were 10°C min^{-1} for heat-treatment temperatures of 300°C, 500°C, and 700°C and 12.8°C min^{-1} for those at 900°C and 1200°C.

Characterization

The crystal structures were determined by X-ray diffractometry (XRD) by using an X-ray diffractometer (D8 ADVANCE, Bruker AXS) with Cu-K_α radiation (λ = 1.5406 Å) and a high-power X-ray diffractometer (HP-XRD; D/MAX2500V/PC, Rigaku). The sample morphologies were investigated using field-emission scanning electron microscopy (FE-SEM; S-4800, Hitachi High-Technologies). High-resolution transmission electron microscopy (HR-TEM; JEOL JEM-2100F TEM system operated at 200 kV) was used to investigate the crystallinity and elemental distribution of the samples. Inductively coupled plasma optical emission spectroscopy (ICP-OES) measurements were conducted using a Varian 700-ES spectrometer to reveal the sample compositions. Thermal analysis was conducted under N_2 flow at a heating rate of 10°C min^{-1} until 1,200°C by using simultaneous differential scanning calorimetry (DSC) and thermogravimetric analysis (TGA) (SDT; Q600, TA instruments). Fourier transform infrared (FTIR) spectroscopy analysis between 4,000 and 400 cm^{-1} was achieved using a Varian 670 spectrometer. An electromechanical Mössbauer spectrometer was used in constant-acceleration mode with a ^{57}Co source in a rhodium matrix, and the sample temperature was maintained at 295 K. The source was accelerated through a range of velocities from −12 to 12 mms^{-1} by using a driving unit to produce the Doppler effect, and the γ-ray energies were scanned. The spectrometer was calibrated at 295 K with a metallic α-Fe foil as the reference absorber. The spectra were analyzed using a least-squares fitting program assuming Lorentzian line shapes. The magnetic properties of the MMOs were measured by using a superconducting quantum interface device-vibrating sample magnetometer (SQUID-VSM). The temperature dependency of the metal cation ratio for each metal cation in the structures was estimated using Equation 1.

$$\textit{Metal cation ratio retention}\ (\%) = \frac{C_{23^\circ C} - |C_T - C_{23^\circ C}|}{C_{23^\circ C}} \times 100 \qquad \text{(Equation 1)}$$

Here, $C_{23°C}$ is the average molar ratio of each metal cation in an LDH sample at 23°C and C_T is the average molar ratio of each metal cation in the samples calcined at temperature T.

SUPPLEMENTAL INFORMATION

Supplemental information can be found online at https://doi.org/10.1016/j.xcrp.2021.100702.

ACKNOWLEDGMENTS

We acknowledge the 2021 Research Fund (1.210035.01) of UNIST (Ulsan National Institute of Science & Technology) for financial support. This work was also supported by the National Research Foundation of Korea (NRF) through a grant funded by the Korean government (MSIT: Ministry of Science and ICT; grant nos. NRF-2018R1C1B6002342, NRF-2019M1A2A2065612, NRF-2021R1C1C2012306, and NRF-2017R1A2B2012241) and the Technology Innovation Program by the Ministry of Trade, Industry & Energy (MOTIE, 20015619).

AUTHOR CONTRIBUTIONS

S.C. proposed, designed, and supervised the research. M.K. synthesized and characterized the samples. W.J. and J.S. contributed to structural characterizations of the samples. I.O. and J.-W.Y. measured the magnetic properties and conducted data analysis. H.C. and C.S.K. obtained the Mössbauer spectra and analyzed the data. M.K., I.O., J.-W.Y., and S.C. co-wrote the manuscript. All authors read and commented on the manuscript.

DECLARATION OF INTERESTS

The authors declare no competing financial interests.

Received: July 8, 2021
Revised: November 1, 2021
Accepted: December 7, 2021
Published: December 29, 2021

REFERENCES

1. Zapata-Solvas, E., Poyato, R., Gómez-García, D., Domínguez-Rodríguez, A., Radmilovic, V., and Padture, N.P. (2008). Creep-resistant composites of alumina and single-wall carbon nanotubes. Appl. Phys. Lett. *92*, 111912.

2. Ndione, P.F., Shi, Y., Stevanovic, V., Lany, S., Zakutayev, A., Parilla, P.A., Perkins, J.D., Berry, J.J., Ginley, D.S., and Toney, M.F. (2014). Control of the Electrical Properties in Spinel Oxides by Manipulating the Cation Disorder. Adv. Funct. Mater. *24*, 610–618.

3. Ndione, P.F., Garcia, A., Widjonarko, N.E., Sigdel, A.K., Steirer, K.X., Olson, D.C., Parilla, P.A., Ginley, D.S., Armstong, N.R., Richards, R.E., et al. (2013). Highly-Tunable Nickel Cobalt Oxide as a Low-Temperature P-Type Contact in Organic Photovoltaic Devices. Adv. Energy Mater. *3*, 524–531.

4. Moya, X., Hueso, L.E., Maccherozzi, F., Tovstolytkin, A.I., Podyalovskii, D.I., Ducati, C., Phillips, L.C., Ghidini, M., Hovorka, O., Berger, A., et al. (2013). Giant and reversible extrinsic magnetocaloric effects in $La_{0.7}Ca_{0.3}MnO_3$ films due to strain. Nat. Mater. *12*, 52–58.

5. Kursumovic, A., Defay, E., Lee, O.J., Tsai, C.-F., Bi, Z., Wang, H., and MacManus-Driscoll, J.L. (2013). A New Material for High-Temperature Lead-Free Actuators. Adv. Funct. Mater. *23*, 5881–5886.

6. Dong, G., Zhou, Z., Guan, M., Xue, X., Chen, M., Ma, J., Hu, Z., Ren, W., Ye, Z.-G., Nan, C.-W., and Liu, M. (2018). Thermal Driven Giant Spin Dynamics at Three-Dimensional Heteroepitaxial Interface in $Ni_{0.5}Zn_{0.5}Fe_2O_4$/$BaTiO_3$-Pillar Nanocomposites. ACS Nano *12*, 3751–3758.

7. MacManus-Driscoll, J.L., Foltyn, S.R., Jia, Q.X., Wang, H., Serquis, A., Civale, L., Maiorov, B., Hawley, M.E., Maley, M.P., and Peterson, D.E. (2004). Strongly enhanced current densities in superconducting coated conductors of $YBa_2Cu_3O_{7-x}$ + $BaZrO_3$. Nat. Mater. *3*, 439–443.

8. Park, C., Wu, R., Lu, P., Zhao, H., Yang, J., Zhang, B., Li, W., Yun, C., Wang, H., MacManus-Driscoll, J.L., and Cho, S. (2018). Use of Mesoscopic Host Matrix to Induce Ferrimagnetism in Antiferromagnetic Spinel Oxide. Adv. Funct. Mater. *28*, 1706220.

9. Cho, S., Yun, C., Kim, Y.S., Wang, H., Jian, J., Zhang, W., Huang, J., Wang, X., Wang, H., and MacManus-Driscoll, J.L. (2018). Strongly enhanced dielectric and energy storage properties in lead-free perovskite titanate thin films by alloying. Nano Energy *45*, 398–406.

10. Pfenninger, R., Struzik, M., Garbayo, I., Stilp, E., and Rupp, J.L.M. (2019). A low ride on processing temperature for fast lithium conduction in garnet solid-state battery films. Nat. Energy *4*, 475–483.

11. Gonzalez-Rosillo, J.C., Balaish, M., Hood, Z.D., Nadkarni, N., Fraggedakis, D., Kim, K.J., Mullin, K.M., Pfenninger, R., Bazant, M.Z., and Rupp, J.L.M. (2020). Lithium-Battery Anode Gains Additional Functionality for Neuromorphic Computing through Metal-Insulator Phase Separation. Adv. Mater. *32*, e1907465.

12. Xia, Y., Xiong, Y., Lim, B., and Skrabalak, S.E. (2009). Shape-controlled synthesis of metal

nanocrystals: simple chemistry meets complex physics? Angew. Chem. Int. Ed. Engl. *48*, 60–103.

13. Khan, A.I., and O'Hare, D. (2002). Intercalation chemistry of layered double hydroxides: recent developments and applications. J. Mater. Chem. *12*, 3191–3198.

14. Sideris, P.J., Nielsen, U.G., Gan, Z., and Grey, C.P. (2008). Mg/Al ordering in layered double hydroxides revealed by multinuclear NMR spectroscopy. Science *321*, 113–117.

15. Clause, O., Rebours, B., Merlen, E., Trifiró, F., and Vaccari, A. (1992). Preparation and characterization of nickel-aluminum mixed oxides obtained by thermal decomposition of hydrotalcite-type precursors. J. Catal. *133*, 231–246.

16. Bellotto, M., Rebours, B., Clause, O., Lynch, J., Bazin, D., and Elkaïm, E. (1996). A Reexamination of Hydrotalcite Crystal Chemistry. J. Phys. Chem. *100*, 8527–8534.

17. Gomes Silva, C., Bouizi, Y., Fornés, V., and García, H. (2009). Layered double hydroxides as highly efficient photocatalysts for visible light oxygen generation from water. J. Am. Chem. Soc. *131*, 13833–13839.

18. Gao, Z., Wang, J., Li, Z., Yang, W., Wang, B., Hou, M., He, Y., Liu, Q., Mann, T., Yang, P., et al. (2011). Graphene Nanosheet/Ni^{2+}/Al^{3+} Layered Double-Hydroxide Composite as a Novel Electrode for a Supercapacitor. Chem. Mater. *23*, 3509–3516.

19. Sumboja, A., Chen, J., Zong, Y., Lee, P.S., and Liu, Z. (2017). NiMn layered double hydroxides as efficient electrocatalysts for the oxygen evolution reaction and their application in rechargeable Zn-air batteries. Nanoscale *9*, 774–780.

20. Zhang, J., Hu, H., Li, Z., and Lou, X.W. (2016). Double-Shelled Nanocages with Cobalt Hydroxide Inner Shell and Layered Double Hydroxides Outer Shell as High-Efficiency Polysulfide Mediator for Lithium-Sulfur Batteries. Angew. Chem. Int. Ed. Engl. *55*, 3982–3986.

21. Zhang, L., Liu, J., Xiao, H., Liu, D., Qin, Y., Wu, H., Li, H., Du, N., and Hou, W. (2014). Preparation and properties of mixed metal oxides based layered double hydroxide as anode materials for dye-sensitized solar cell. Chem. Eng. J. *250*, 1–5.

22. Yin, Z., Wu, J., and Yang, Z. (2011). Amperometric sensors based on Ni/Al and Co/Al layered double hydroxides modified electrode and their application for hydrogen peroxide detection. Biosens. Bioelectron. *26*, 1970–1974.

23. Long, X., Wang, Z., Xiao, S., An, Y., and Yang, S. (2016). Transition metal based layered double hydroxides tailored for energy conversion and storage. Mater. Today *19*, 213–226.

24. Bellotto, M., Rebours, B., Clause, O., Lynch, J., Bazin, D., and Elkaïm, E. (1996). Hydrotalcite Decomposition Mechanism: A Clue to the Structure and Reactivity of Spinel-like Mixed Oxides. J. Phys. Chem. *100*, 8535–8542.

25. Ma, Y., Ma, Y., Wang, Q., Schweidler, S., Botros, M., Fu, T., Hahn, H., Brezesinski, T., and Breitung, B. (2021). High-entropy energy materials: Challenges and new opportunities. Energy Environ. Sci. *14*, 2883–2905.

26. George, E.P., Raabe, D., and Ritchie, R.O. (2019). High-entropy alloys. Nat. Rev. Mater. *4*, 515–534.

27. Song, B., Yang, Y., Rabbani, M., Yang, T.T., He, K., Hu, X., Yuan, Y., Ghildiyal, P., Dravid, V.P., Zachariah, M.R., et al. (2020). In situ oxidation studies of high-entropy alloy nanoparticles. ACS Nano *14*, 15131–15143.

28. Sarkar, A., Wang, Q., Schiele, A., Chellali, M.R., Bhattacharya, S.S., Wang, D., Brezesinski, T., Hahn, H., Velasco, L., and Breitung, B. (2019). High-entropy oxides: Fundamental aspects and electrochemical properties. Adv. Mater. *31*, e1806236.

29. Rost, C.M., Sachet, E., Borman, T., Moballegh, A., Dickey, E.C., Hou, D., Jones, J.L., Curtarolo, S., and Maria, J.-P. (2015). Entropy-stabilized oxides. Nat. Commun. *6*, 8485.

30. Chen, H., Qiu, N., Wu, B., Yang, Z., Sun, S., and Wang, Y. (2020). A new spinel high-entropy oxide $(Mg_{0.2}Ti_{0.2}Zn_{0.2}Cu_{0.2}Fe_{0.2})_3O_4$ with fast reaction kinetics and excellent stability as an anode material for lithium ion batteries. RSC Advances *10*, 9736–9744.

31. Sarker, P., Harrington, T., Toher, C., Oses, C., Samiee, M., Maria, J.-P., Brenner, D.W., Vecchio, K.S., and Curtarolo, S. (2018). High-entropy high-hardness metal carbides discovered by entropy descriptors. Nat. Commun. *9*, 4980.

32. Zhang, L., Cai, W., and Bao, N. (2021). Top-level design strategy to construct an advanced high-entropy Co–Cu–Fe–Mo (oxy)hydroxide electrocatalyst for the oxygen evolution reaction. Adv. Mater. *33*, e2100745.

33. Glasscott, M.W., Pendergast, A.D., Goines, S., Bishop, A.R., Hoang, A.T., Renault, C., and Dick, J.E. (2019). Electrosynthesis of high-entropy metallic glass nanoparticles for designer, multi-functional electrocatalysis. Nat. Commun. *10*, 2650.

34. Jin, Z., Lv, J., Jia, H., Liu, W., Li, H., Chen, Z., Lin, X., Xie, G., Liu, X., Sun, S., and Qiu, H.J. (2019). Nanoporous Al-Ni-Co-Ir-Mo high-entropy alloy for record-high water splitting activity in acidic environments. Small *15*, e1904180.

35. Wang, J., Stenzel, D., Azmi, R., Najib, S., Wang, K., Jeong, J., Sarkar, A., Wang, Q., Sukkurji, P.A., Bergfeldt, T., et al. (2020). Spinel to rock-salt transformation in high entropy oxides with Li incorporation. Electrochem *1*, 60–74.

36. Lacey, S.D., Dong, Q., Huang, Z., Luo, J., Xie, H., Lin, Z., Kirsch, D.J., Vattipalli, V., Povinelli, C., Fan, W., et al. (2019). Stable multimetallic nanoparticles for oxygen electrocatalysis. Nano Lett. *19*, 5149–5158.

37. Fang, G., Gao, J., Lv, J., Jia, H., Li, H., Liu, W., Xie, G., Chen, Z., Huang, Y., Yuan, Q., et al. (2020). Multi-component nanoporous alloy/(oxy)hydroxide for bifunctional oxygen electrocatalysis and rechargeable Zn-air batteries. Appl. Catal. B *268*, 118431.

38. Ghigna, P., Airoldi, L., Fracchia, M., Callegari, D., Anselmi-Tamburini, U., D'Angelo, P., Pianta, N., Ruffo, R., Cibin, G., de Souza, D.O., and Quartarone, E. (2020). Lithiation mechanism in high-entropy oxides as anode materials for Li-Ion batteries: An operando XAS study. ACS Appl. Mater. Interfaces *12*, 50344–50354.

39. Jenkins, H.D.B., Roobottom, H.K., Passmore, J., and Glasser, L. (1999). Relationships among Ionic Lattice Energies, Molecular (Formula Unit) Volumes, and Thermochemical Radii. Inorg. Chem. *38*, 3609–3620.

40. Labajos, F.M., Rives, V., and Ulibarri, M.A. (1992). Effect of hydrothermal and thermal treatments on the physicochemical properties of Mg-Al hydrotalcite-like materials. J. Mater. Sci. *27*, 1546–1552.

41. Kloprogge, J.T., and Frost, R.L. (1999). Fourier Transform Infrared and Raman Spectroscopic Study of the Local Structure of Mg-, Ni-, and Co-Hydrotalcites. J. Solid State Chem. *146*, 506–515.

42. Chen, W., and Qu, B. (2003). Structural Characteristics and Thermal Properties of PE-g-MA/MgAl-LDH Exfoliation Nanocomposites Synthesized by Solution Intercalation. Chem. Mater. *15*, 3208–3213.

43. Ahmed, A.A.A., Talib, Z.A., bin Hussein, M.Z., and Zakaria, A. (2012). Zn–Al layered double hydroxide prepared at different molar ratios: Preparation, characterization, optical and dielectric properties. J. Solid State Chem. *191*, 271–278.

44. Karami, Z., Jouyandeh, M., Ali, J.A., Ganjali, M.R., Aghazadeh, M., Maadani, M., Rallini, M., Luzi, F., Torre, L., Puglia, D., and Saeb, M.R. (2019). Development of Mg-Zn-Al-CO_3 ternary LDH and its curability in epoxy/amine system. Prog. Org. Coat. *136*, 105264.

45. Arizaga, G.G.C., Gardolinski, J.E.F.C., Schreiner, W.H., and Wypych, F. (2009). Intercalation of an oxalatooxoniobate complex into layered double hydroxide and layered zinc hydroxide nitrate. J. Colloid Interface Sci. *330*, 352–358.

46. Marchi, A.J., and Apesteguía, C.R. (1998). Impregnation-induced memory effect of thermally activated layered double hydroxides. Appl. Clay Sci. *13*, 35–48.

47. Jeong, I.R., Lee, J.H., Song, J., Oh, Y.S., and Cho, S. (2020). Control of structural disorder in spinel ceramics derived from layered double hydroxides. Ceram. Int. *46*, 6594–6599.

48. O'Neill, H.S.C., and Navrotsky, A. (1983). Simple spinels: crystallographic parameters, cation radii, lattice energies, and cation distribution. Am. Mineral. *68*, 181–194.

49. Lavina, B., Salviulo, G., and Della Giusta, A. (2002). Cation distribution and structure modelling of spinel solid solutions. Phys. Chem. Miner. *29*, 10–18.

50. Faungnawakij, K., Shimoda, N., Fukunaga, T., Kikuchi, R., and Eguchi, K. (2008). Cu-based spinel catalysts CuB_2O_4 (B = Fe, Mn, Cr, Ga, Al, $Fe_{0.75}Mn_{0.25}$) for steam reforming of dimethyl ether. Appl. Catal. A Gen. *341*, 139–145.

51. Dąbrowa, J., Stygar, M., Mikuła, A., Knapik, A., Mroczka, K., Tejchman, W., Danielewski, M., and Martin, M. (2018). Synthesis and microstructure of the $(Co,Cr,Fe,Mn,Ni)_3O_4$ high entropy oxide characterized by spinel structure. Mater. Lett. *216*, 32–36.

52. Navrotsky, A., and Kleppa, O.J. (1968). Thermodynamics of formation of simple spinels. J. Inorg. Nucl. Chem. *30*, 479–498.

53. Starukh, G., Rozovik, O., and Oranska, O. (2016). Organo/Zn-Al LDH Nanocomposites for Cationic Dye Removal from Aqueous Media. Nanoscale Res. Lett. *11*, 228.

54. Benito, P., Guinea, I., Labajos, F.M., Rocha, J., and Rives, V. (2008). Microwave-hydrothermally aged Zn,Al hydrotalcite-like compounds: Influence of the composition and the irradiation conditions. Microporous Mesoporous Mater. *110*, 292–302.

55. Ferragina, P., and Manzini, G. (2000). Opportunistic data structures with applications. Proceedings 41st Annual Symposium on Foundations of Computer Science, pp. 390–398.

56. Yan, K., Liu, Y., Lu, Y., Chai, J., and Sun, L. (2017). Catalytic application of layered double hydroxide-derived catalysts for the conversion of biomass-derived molecules. Catal. Sci. Technol. *7*, 1622–1645.